# Modeling uncertainties of $t\bar{t}W^{\pm}$ multilepton signatures

G. Bevilacqua[1], H. Y. Bi[2], F. Febres Cordero[3], H. B. Hartanto[4], M. Kraus[3], J. Nasufi[2],
L. Reina[3], and M. Worek[2]

[1]*ELKH-DE Particle Physics Research Group, University of Debrecen,*
*H-4010 Debrecen, P.O. Box 105, Hungary*
[2]*Institute for Theoretical Particle Physics and Cosmology, RWTH Aachen University,*
*D-52056 Aachen, Germany*
[3]*Physics Department, Florida State University, Tallahassee, Florida 32306-4350, USA*
[4]*Cavendish Laboratory, University of Cambridge, J.J. Thomson Avenue,*
*Cambridge CB3 0HE, United Kingdom*

In light of recent discrepancies between the modeling of $t\bar{t}W^{\pm}$ signatures and measurements reported by the LHC experimental collaborations, we investigate in detail theoretical uncertainties for multilepton signatures. We compare results from the state-of-the-art full off-shell calculation and its narrow-width approximation to results obtained from the on-shell $t\bar{t}W^{\pm}$ calculation, with approximate spin correlations in top-quark and $W$ decays, matched to parton showers. In the former case double-, single-, and nonresonant contributions together with interference effects are taken into account, while the latter two cases are only based on the double-resonant top-quark contributions. The comparison is performed for the LHC at $\sqrt{s} = 13$ TeV for which we study separately the multilepton signatures as predicted from the dominant next-to-leading-order (NLO) contributions at the perturbative orders $\mathcal{O}(\alpha_s^3\alpha^6)$ and $\mathcal{O}(\alpha_s\alpha^8)$. Furthermore, we combine both contributions and propose a simple way to approximately incorporate the full off-shell effects in the NLO computation of on-shell $pp \to t\bar{t}W^{\pm}$ matched to parton showers.

## I. INTRODUCTION

The hadronic production of top-quark pairs in association with a $W$ boson is one of the most massive signatures currently accessible at the LHC and allows us to study possible deviations from the Standard Model (SM) dynamics of top quarks in the presence of charged electroweak (EW) gauge bosons. As the accompanying top quarks are rapidly decaying into a $W$ boson and a $b$ quark, the signature of the $pp \to t\bar{t}W^{\pm}$ process involves two $b$ jets and the subsequent decay pattern of three decaying $W$ bosons. This gives rise to the rare Standard Model production of same-sign lepton pairs and other multilepton signatures that are relevant to a multitude of searches [1–4] for physics beyond the Standard Model as well as to the measurement of Higgs-boson production in association with a top-quark pair [5–8] and of four top-quarks [9–12].

Because of the importance of the $pp \to t\bar{t}W^{\pm}$ process to validate the EW interactions of the top quark and as a

dominant background to many ongoing measurements and searches at the LHC, it is crucial to have the process under excellent theoretical control. Interestingly, small tensions between the $t\bar{t}W$ measurements and the SM predictions have been reported since its discovery. The first measurements [13,14] during the LHC Run 1 at a center-of-mass energy of $\sqrt{s} = 8$ TeV already reported tensions for the measured cross section slightly above the $1\sigma$ level. Further measurements [15–17] performed at $\sqrt{s} = 13$ TeV confirmed the picture that a slight excess of $t\bar{t}W$ events is observed. Additional measurements of the $t\bar{t}W$ cross section [7,8,10,11], from analyses aimed at the measurement of $t\bar{t}H$ and $t\bar{t}t\bar{t}$ production and utilizing data corresponding to an integrated luminosity of up to $\mathcal{L} = 139$ fb$^{-1}$, still see a persisting tension with respect to the corresponding SM predictions depending on the considered final-state signature, where the largest deviation of up to a factor of 1.7 has been found in multilepton signatures [7].

Fueled by these deviations, tremendous progress has been made in the last decade in the theoretical description of the $pp \to t\bar{t}W^{\pm}$ processes. The first next-to-leading (NLO) QCD corrections have been computed in Refs. [18,19], while EW contributions have been investigated in Refs. [20–22]. Furthermore, the resummation of soft gluon effects at the next-to-next-to-leading logarithmic

level has been achieved recently in Refs. [23–27]. Targeting a more realistic description of fiducial signatures, the $t\bar{t}W^{\pm}$ process has been matched to parton showers (PS) either using the MC@NLO matching scheme [28,29] in Refs. [30–32] or the POWHEG method [33,34] in Refs. [35,36]. The impact of higher-order corrections via multijet merging has been studied as well in Refs. [37–39]. In parallel, also, the inclusion of off-shell effects for top quarks and $W$ bosons as well as single- and nonresonant contributions together with interference effects have been studied including NLO QCD corrections [40–42] as well as complete NLO SM corrections [43].

The emergent picture from all the aforementioned studies is that NLO QCD corrections are of the order of 8%–20% depending on the chosen SM input parameters and cuts applied on the final states. The resummation of soft gluon effects in on-shell $t\bar{t}W$ production improves only marginally the perturbative convergence of NLO QCD predictions and increases the rate by less than 10%. The second largest contribution in the perturbative expansion of the cross section comprises the NLO QCD corrections to the pure EW born and amounts roughly to a +10% correction to the total NLO cross section. Including higher-order corrections via multijet merging also increases the inclusive cross section by a similar amount. On the other hand, QCD corrections to top-quark decays are negative and decrease the production rate by roughly 5%. Finally, even though off-shell effects and nonresonant contributions are small at the integrated level, they become sizable in the tails of dimensionful observables where they can make a difference even up to 70%. Overall, none of the effects described above can fully explain the tension between the measurements and the SM prediction. However, given the complexity of the signatures involved and the progress made to theoretically model them at both the integrated and differential fiducial levels, a study aimed at comparing existing computations and understanding the origin of their differences as well as the individual residual uncertainties is of the utmost importance to eventually propose a theory recommendation for the comparison with data.

As existing computations are often quite different in nature and therefore inherently affected by distinctive theoretical uncertainties, it is not evident how to combine the various findings into a precise modeling of the $t\bar{t}W$ process. In this paper, we attempt to do a first comparison between parton-shower matched predictions and fixed-order full off-shell calculations, together with their corresponding narrow-width approximations (NWAs), in order to understand the different approaches in more detail. In all cases, we include NLO QCD corrections to both the QCD and EW born level, in the following simply denoted by QCD and EW (see Sec. II). Incidentally, we also quantify for the first time the size of full off-shell effects for the EW contribution. Our comparison focuses on the multilepton

signature as it is not only the cleanest signature on the theoretical side but also yields the strongest discrepancies when compared to measurements.

The paper is organized as follows. In Sec. II, we summarize the computational setup of the calculations employed in our study, while in Sec. III, we highlight in detail the differences between the various theoretical approaches. In Sec. IV, we study the modeling of top-quark production and decays separately for the QCD and EW contributions. In Sec. V, we show our phenomenological results and propose a simple method to approximately capture the full off-shell effects in parton-shower matched calculations for on-shell $t\bar{t}W^{\pm}$ production. Finally, we give our conclusions in Sec. VI.

## II. COMPUTATIONAL SETUP

In our study, we consider the $pp \to \ell^+\nu\ell^-\nu\ell^{\pm}\nu b\bar{b}$ process at $\mathcal{O}(\alpha_s^3\alpha^6)$ and $\mathcal{O}(\alpha_s\alpha^8)$, where $\ell = e, \mu$ and all possible lepton-flavor combinations are considered. In the following, we will refer to the former perturbative order as $t\bar{t}W^{\pm}$ QCD and the latter as $t\bar{t}W^{\pm}$ EW. We will provide predictions for the LHC operating at a center-of-mass energy of $\sqrt{s} = 13$ TeV and parametrize the proton content using the NNPDF3.1 [44] parton distribution function (PDF) set as provided by the LHAPDF interface [45]. We employ the necessary SM input parameters in the $G_F$ input scheme [46]. For the electroweak bosons, we choose the following masses and corresponding decay widths:

$$M_W = 80.3850 \text{ GeV}, \qquad \Gamma_W = 2.09767 \text{ GeV},$$

$$M_Z = 91.1876 \text{ GeV}, \qquad \Gamma_Z = 2.50775 \text{ GeV},$$

$$M_H = 125.000 \text{ GeV}, \qquad \Gamma_H = 0.00407 \text{ GeV}. \tag{1}$$

Together with the Fermi constant $G_F = 1.166378 \times 10^{-5} \text{ GeV}^{-2}$, the electromagnetic coupling is given by

$$\alpha = \frac{\sqrt{2}}{\pi} G_F M_W^2 \left(1 - \frac{M_W^2}{M_Z^2}\right). \tag{2}$$

Finally, we choose for the top-quark mass

$$m_t = 172.5 \text{ GeV}. \tag{3}$$

We postpone the discussion of the top-quark width as it depends on the approximation used in the corresponding calculation. Let us now turn to the description of the various theoretical predictions employed in our study.

*Full off-shell:* Using the HELAC-NLO framework [47–53] we generate results at fixed-order NLO QCD accuracy, employing the matrix elements for the fully decayed final state $pp \to \ell^+\nu\ell^-\nu\ell^{\pm}\nu b\bar{b}$ at $\mathcal{O}(\alpha_s^3\alpha^6)$ and $\mathcal{O}(\alpha_s\alpha^8)$. This approach includes all double-, single-, and nonresonant top-quark and $W$-boson contributions as well as interference and spin-correlation effects at the

matrix element level. Top quarks and electroweak gauge bosons are described in the complex-mass scheme [46,54,55] by Breit-Wigner propagators. Therefore, the top-quark decay width is calculated at NLO QCD accuracy including off-shell $W$ bosons according to formulas given in Refs. [56–58], which for our study corresponds to

$$\Gamma^{\text{NLO}}_{t,\text{off-shell}} = 1.33247 \text{ GeV}. \qquad (4)$$

Bottom quarks are treated consistently as massless quarks throughout the computation. The renormalization and factorization scales are chosen as

$$\mu_0 = \frac{H_T}{3}, \quad \text{with} \quad H_T = \sum_{i=1}^{3} p_T(\ell_i) + \sum_{i=1}^{2} p_T(b_i) + p_T^{\text{miss}}. \qquad (5)$$

More details on the calculation can be found in Ref. [40].

*NWA:* Benefiting from the recent automation of the NWA in the HELAC-NLO framework [59], we are able to provide results at NLO QCD accuracy including spin-correlated top-quark decays. In this approach, the full matrix elements for $pp \to \ell^+\nu\ell^-\bar{\nu}\ell^{\pm}\nu b\bar{b}$ are approximated by the double-resonant $t\bar{t}W^{\pm}$ contributions via a factorization of the cross section into a production and a decay stage by applying the following relation to top-quark and $W$-boson propagators:

$$\lim_{\Gamma/m \to 0} \frac{1}{(p^2 - m^2)^2 + m^2\Gamma^2} = \frac{\pi}{m\Gamma}\delta(p^2 - m^2) + \mathcal{O}\left(\frac{\Gamma}{m}\right). \qquad (6)$$

In this limit, the cross section can be written as

$$\begin{aligned} d\sigma_{\text{NWA}} = {}&d\sigma_{pp \to t\bar{t}W^{\pm}} \otimes d\mathcal{B}_{t \to bW^+} \otimes d\mathcal{B}_{\bar{t} \to \bar{b}W^-} \\ &\otimes d\mathcal{B}_{W^+ \to \ell^+\nu} \otimes d\mathcal{B}_{W^- \to \ell^-\nu} \otimes d\mathcal{B}_{W^{\pm} \to \ell^{\pm}\nu}, \end{aligned} \qquad (7)$$

where $\mathcal{B}$ denotes the corresponding branching ratios and $\otimes$ indicates that full spin correlations are kept. The computation is tremendously simplified with respect to the full off-shell calculation but still allows us to systematically include NLO QCD corrections separately in the production and decay stages. In this case, the top-quark decay width is given by

$$\Gamma^{\text{NLO}}_{t,\text{NWA}} = 1.35355 \text{ GeV}. \qquad (8)$$

If QCD corrections to the top-quark decay are omitted, which we denote as "NWA LO decay", we use the

leading-order (LO) prediction for the top-quark width given by

$$\Gamma^{\text{LO}}_{t,\text{NWA}} = 1.48063 \text{ GeV}. \qquad (9)$$

For the renormalization and factorization scales, we choose as before

$$\mu_0 = \frac{H_T}{3}. \qquad (10)$$

POWHEG-BOX: We employ parton-shower matched results for $pp \to t\bar{t}W^{\pm}$ using the recent POWHEG-BOX implementation presented in Ref. [36], based on one-loop amplitudes provided via NLOX [60,61]. In this calculation, the on-shell production of $t\bar{t}W^{\pm}$ is matched to parton showers at NLO accuracy, meaning that NLO QCD corrections are only included in the production stage. The renormalization and factorization scales are chosen according to

$$\mu_0 = \frac{E_T}{3}. \quad \text{with} \quad E_T = \sum_{i \in \{t,\bar{t},W\}} \sqrt{m_i^2 + p_{T,i}^2}. \qquad (11)$$

In the matching procedure, the POWHEG-BOX employs two damping parameters, $h_{\text{damp}}$ and $h_{\text{bornzero}}$, to define a jet function that classifies the soft and hard real contributions. Based on the results of Ref. [36], in this study, we choose the central values

$$h_{\text{damp}} = \frac{E_T}{2}, \qquad h_{\text{bornzero}} = 5$$

and estimate the dependence of our results on these parameters by varying their values independently in the ranges

$$h_{\text{damp}} = \left\{\frac{E_T}{4}, \frac{E_T}{2}, E_T\right\}, \quad \text{and} \quad h_{\text{bornzero}} = \{2, 5, 10\}. \qquad (12)$$

The decay of the top quarks and the $W$ bosons are included at LO accuracy using the method introduced in Ref. [62] that allows us to retain spin correlations and to introduce a smearing of top-quark and $W$ boson virtualities according to Breit-Wigner distributions. However, single- and nonresonant top-quark and $W$-boson contributions are still missing. They are not included even with LO accuracy. As the decay modeling in the POWHEG-BOX does not follow any particular fixed-order scheme, we use the LO top-quark width including off-shell effects for the $W$ boson,

$$\Gamma^{\text{LO}}_{t,\text{off-shell}} = 1.45759 \text{ GeV}. \tag{13}$$

However, the top-quark decay width enters only the decay chain matrix elements which employ Breit-Wigner propagators; see Ref. [36]. Thus, the chosen value of $\Gamma_t$ has generally a very small impact on our results. We employ NLO accurate branching ratios for the $W$-boson decays to be consistent with the full off-shell calculation. Thus, the total leptonic branching ratio is given by

$$\text{Br}(W \to \ell\nu) = \sum_{i=1}^{3} \frac{\Gamma(W \to \ell_i\nu_i)}{\Gamma_W^{\text{NLO}}} = 0.325036. \tag{14}$$

MG5_aMC@NLO: We also use parton-shower matched computations for the on-shell $pp \to t\bar{t}W^{\pm}$ process in the MC@NLO framework as provided by MG5_aMC@NLO [63]. This approach has the same formal accuracy as the aforementioned POWHEG-BOX computation. The renormalization and factorization scales are also chosen as

$$\mu_0 = \frac{E_T}{3}, \tag{15}$$

where $E_T$ is defined in Eq. (11),[1] while the initial shower scale $\mu_Q$ is left to the default option

$$\mu_Q = \frac{1}{2} \sum_{i \in \{t,\bar{t},W,j\}} \sqrt{m_i^2 + p_{T,i}^2}. \tag{16}$$

We study the dependence of our results on the initial shower scale $\mu_Q$ by varying it up and down by a factor of 2. LO spin-correlated top-quark and $W$-boson decays are included via MADSPIN [64] that automates the approach of Ref. [62]. Within MADSPIN, the necessary branching ratios are evaluated at leading-order accuracy by default. However, we rescale our results to be consistent with Eq. (14) as discussed in the next section.

In all cases, we choose for the renormalization and factorization scales

$$\mu_R = \mu_F = \mu_0, \tag{17}$$

where the specific choice of $\mu_0$ in each computational framework considered has been discussed above. The dependence on the scale choice is estimated from

independent variations of renormalization and factorization scales in the range of

$$\left(\frac{\mu_R}{\mu_0}, \frac{\mu_F}{\mu_0}\right) = \{(0.5, 0.5), (0.5, 1), (1, 0.5), (1, 1),$$
$$(1, 2), (2, 1), (2, 2)\}. \tag{18}$$

By searching for the minimum and the maximum of the resulting cross sections, one obtains an uncertainty band.

For the parton-shower matched predictions, we generate Les Houches event files [65,66] that are subsequently showered with PYTHIA8 [67,68]. In the parton-shower evolution, we do not take into account hadronization effects and multiple parton interactions. The analysis of showered events is then performed within the RIVET framework [69,70] that also provides an interface to FASTJET [71,72].

Because of the complexity of the full off-shell computation, we store our theoretical predictions obtained with the HELAC-NLO framework in the form of events, available in either the format of modified Les Houches event files [66] or ROOT Ntuples [73]. Based on ideas presented in Ref. [74], events are stored with additional information about matrix elements and PDFs. We improve the performance of our framework by storing partially unweighted events; see, e.g., Ref. [75] for more information. The Ntuples allow for on-the-fly reweighting for different PDF sets or scale choices as well as studying different fiducial phase space cuts. The reweighting and event analysis is performed within HEPLOT [76].

The shower input cards, the RIVET analysis code, and all histogram data are made available in the Supplemental Material [77].

### III. DIFFERENCES OF THE VARIOUS COMPUTATIONAL APPROACHES

Before presenting our phenomenological results, we want to discuss the intrinsic differences between the various computational approaches introduced above.

Let us start with the purely technical issue of choosing renormalization and factorization scales $\mu_0$ for the various approaches. To obtain a good perturbative convergence for dimensionful observables, a dynamic-scale choice has to be employed. However, because of the nature of the different approaches, we cannot use a common scale choice. For instance, the off-shell and NWA predictions use scales evaluated on the momenta of the fully decayed final state, while parton-shower-based predictions use the on-shell momenta of the intermediate unstable particles. We checked explicitly that our conclusions in the following sections do not depend significantly on the scale chosen. Specifically, we performed a comparison using the fixed-scale $\mu_0 = m_t + m_W/2$ that can be employed in all predictions. Shape differences of differential distributions, induced by the dynamic scale choices, are common in

---

[1]The default dynamical scale choice for the renormalization and factorization scales in the POWHEG-BOX and in MG5_aMC@NLO actually corresponds to the definition of Eq. (16). We noticed that our choice of Eq. (11) increases the total cross section by approximately 11%, which is within the estimated scale uncertainties, as we will see later on.
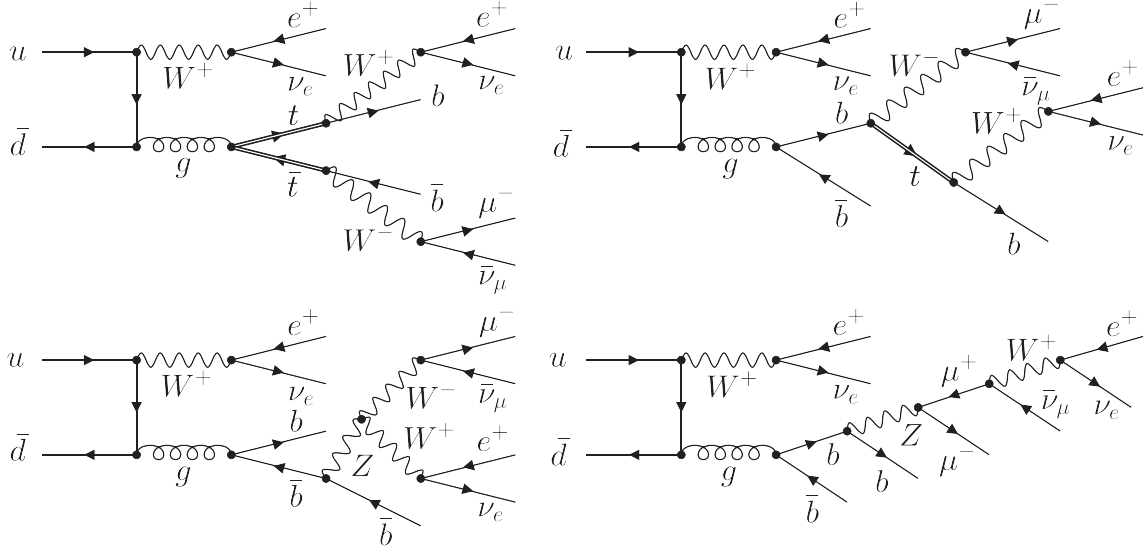
FIG. 1. Representative Feynman diagrams of the double-, single-, and nonresonant top-quark contributions that are part of the matrix elements employed in the full off-shell computation. Feynman diagrams were produced with the help of the FEYNGAME program [78].

magnitude, and for all predictions, they are independent of the specific definition of the scale.

Next, we want to discuss differences that affect predominantly the overall normalization of the predictions. First, we focus on differences between MG5_aMC@NLO and the POWHEG-BOX. The inclusive cross section for the three-lepton signature, as predicted by parton-shower matched calculations, is given in terms of production cross section times branching ratios

$$\sigma_{3\ell}^{\mathrm{NLO+PS}} = \sigma(pp \to t\bar{t}W^{\pm}) \times \mathrm{Br}(t \to W^+b)\mathrm{Br}(\bar{t} \to W^-\bar{b})$$
$$\times 8[\mathrm{Br}(W^{\pm} \to \ell_i\nu_i)]^3, \qquad (19)$$

where the factor 8 accounts for all combinations of $\ell = e,\ \mu$. In parton-shower-based predictions, the top-quark decays always into a $W$ boson and a $b$ quark; thus, the branching ratio is $\mathrm{Br}(t \to Wb) = 1$ and drops out from any inclusive or fiducial cross section. In other words, the obtained cross section is completely independent of $\Gamma_t$, even in fiducial phase space volumes. However, the cross section is very sensitive to the branching ratio for the leptonic decay width of the $W$ boson as it depends on it cubicly. In MADSPIN, all branching ratios are computed at LO accuracy from the given input parameters. On the other hand, in the POWHEG-BOX, the total leptonic $W$ boson branching ratio is an independent input parameter that we set to the NLO value. The difference between LO and NLO branching ratios is only of the order of 2.5%. Nonetheless, because of the strong dependence of the cross section on this parameter, we observe a $\mathcal{O}(10\%)$ higher cross section if LO branching ratios are employed. To obtain a cleaner comparison, we rescale the MG5_aMC@NLO predictions globally by a factor of

$$\left(\frac{\mathrm{Br}^{\mathrm{NLO}}(W^{\pm} \to \ell_i\nu_i)}{\mathrm{Br}^{\mathrm{LO}}(W^{\pm} \to \ell_i\nu_i)}\right)^3 \approx 0.92716\dots. \qquad (20)$$

Considering next the NWA approach, we observe that in this case the cross section depends globally on the top-quark decay width via $1/\Gamma_t^2$. Therefore, contrary to parton-shower-based calculation, the inclusive cross section depends crucially on the chosen value of $\Gamma_t$. Moreover, to ensure consistency in the comparison between full off-shell results and predictions in the NWA, the unexpanded NWA results are used. We have studied in Ref. [40] that the impact of these higher-order terms is at the level of 3%–4%.

With respect to the NWA, the full off-shell calculation includes additional contributions. Besides the double-resonant $pp \to t\bar{t}W^{\pm}$ production, the off-shell matrix elements also receive contributions from single-resonant $pp \to tWWb$ and nonresonant $pp \to WWWb\bar{b}$ production modes as well as their interferences. We show some representative Feynman diagrams for each contribution in Fig. 1. We want to stress, however, that the single- and nonresonant production cross sections cannot be computed separately in a gauge-invariant way, as these processes start to mix once higher-order corrections are included. Therefore, the only unambiguous way to account for these contributions is to employ the full matrix elements for $pp \to \ell^+\nu\ell^-\nu\ell^{\pm}\nu b\bar{b}$. Notice that the $\Gamma_t$ dependence in the full off-shell computation is due to Breit-Wigner propagators of the double- and single-resonant contributions.

Finally, the last conceptual difference between the fixed-order computations and the parton-shower predictions concerns the definition of $b$ jets. The fixed-order computations are performed in the five-flavor scheme, treating $b$ quarks as massless. In this case, we define the $b$-jet flavor

using the net *bottomness* in a jet, according to the recombination rules

$$bg \to b, \qquad \bar{b}g \to \bar{b}, \qquad b\bar{b} \to g, \qquad (21)$$

which renders the jet-flavor definition infrared safe at NLO. Beyond NLO, the flavored $k_T$-jet algorithm of Ref. [79] is the most adopted solution to define the flavor of jets for massless partons. Recently, a flavored anti-$k_T$ jet algorithm has also been introduced [80]. On the other hand, the $b$ quark is treated as a massive quark in the parton-shower evolution. As the collinear divergence in the $g \to b\bar{b}$ splitting is regulated by the bottom-quark mass, we can define a $b$ jet to be a jet that has at least one $b$ quark among its constituents. Hadronization effects can have an impact on the definition of $b$-jet observables. However, in preliminary calculations where we included hadronization effects, we only found marginal differences for the considered $b$-jet observables. We have also checked explicitly that a parton-shower evolution with massless $b$ quarks but employing the jet algorithm of Ref. [79][2] yields results that are very similar to the default approach of massive $b$ quarks clustered via the anti-$k_T$ jet algorithm.

## IV. PHENOMENOLOGICAL RESULTS

For our comparison, we focus on the three-lepton signature, where we exclude $\tau$ leptons, as their decays produce very distinct signatures and can be easily distinguished from electron or muon final states. Jets are formed using the anti-$k_T$ jet algorithm [81] with a separation parameter $R = 0.4$. We require at least two $b$ jets that satisfy the conditions

$$p_T(j_b) > 25 \text{ GeV}, \qquad |\eta(j_b)| < 2.5. \qquad (22)$$

Furthermore, we require the presence of exactly three charged leptons with

$$p_T(\ell) > 25 \text{ GeV}, \qquad |\eta(\ell)| < 2.5,$$
$$\Delta R(\ell\ell) > 0.4, \qquad \Delta R(\ell j_b) > 0.4. \qquad (23)$$

Note that in our case the three charged leptons always consist of a two-same-sign lepton pair $\ell\ell^{ss}$ and a single lepton with opposite charge $\ell^{os}$.

### A. QCD production of $t\bar{t}W^{\pm}$

We start our discussion with the dominant QCD production mechanism for the $pp \to t\bar{t}W^{\pm}$ process and its leptonic decay at $\mathcal{O}(\alpha_s^3 \alpha^6)$.

---

[2]We thank Gavin Salam for providing us with his private implementation of the flavor-$k_T$ jet algorithm in FASTJET.

### 1. Integrated fiducial cross sections

First, we present a comparison of fiducial cross sections and their uncertainties. For the off-shell calculation, we obtain

$$\sigma_{\text{off-shell}}^{\text{NLO}} = 1.58^{+0.05(3\%)}_{-0.10(6\%)} \text{ fb}, \qquad (24)$$

which shows a very reduced sensitivity to the choice of the renormalization and factorization scales with changes only between $+3\%$ and $-6\%$ around the central prediction. We do not investigate PDF uncertainties here, since these have already been addressed in Ref. [40] and were estimated to be of the order of 2%–3% depending on the PDF set used. For the NWA with and without NLO QCD corrections to the top-quark decays, we obtain

$$\sigma_{\text{NWA}}^{\text{NLO}} = 1.57^{+0.05(3\%)}_{-0.10(6\%)} \text{ fb}, \qquad \sigma_{\text{NWALODec}}^{\text{NLO}} = 1.66^{+0.17(10\%)}_{-0.17(10\%)} \text{ fb}. \qquad (25)$$

We observe that the full NWA is in perfect agreement with the off-shell prediction. However, if QCD corrections to top-quark decays are neglected, we obtain a 5% larger cross section, and the residual scale sensitivity increases up to $\pm 10\%$. Finally, for the parton-shower matched computations, we find

$$\sigma_{\text{PWG}}^{\text{NLO+PS}} = 1.40^{+0.16(11\%)}_{-0.15(11\%)} \text{ fb}, \qquad \sigma_{\text{MG5}}^{\text{NLO+PS}} = 1.40^{+0.16(11\%)}_{-0.15(11\%)} \text{ fb}. \qquad (26)$$

The remarkable agreement between the two predictions is not a coincidence since we have corrected for the different values of branching ratios employed in the calculations (see Sec. III) and have aligned as much as possible PYTHIA8 parameters between MG5_aMC@NLO and the POWHEG-BOX. The parton-shower matched computations predict a 11% smaller cross section if compared to the off-shell result. The reduction of the cross section is due to multiple emissions in the top-quark decays that are not clustered back into the corresponding $b$ jet and thus decrease the amount of events passing our selection cuts. We checked explicitly that if we turn off parton-shower emissions in the decays we obtain a larger cross section, closer to the result of the NWA with LO decays. Finally, the NLO + PS results show, similar to the NWA LO-decay result, a scale sensitivity of the order of $\pm 11\%$, as expected since both computations include NLO QCD corrections only in the production part of the $pp \to t\bar{t}W^{\pm}$ processes.

### 2. Differential distributions

At the differential level, we start by comparing hadronic $b$-jet observables. All observables are shown as plots containing three panels. The upper panel always depicts the central differential distribution (i.e., the distribution
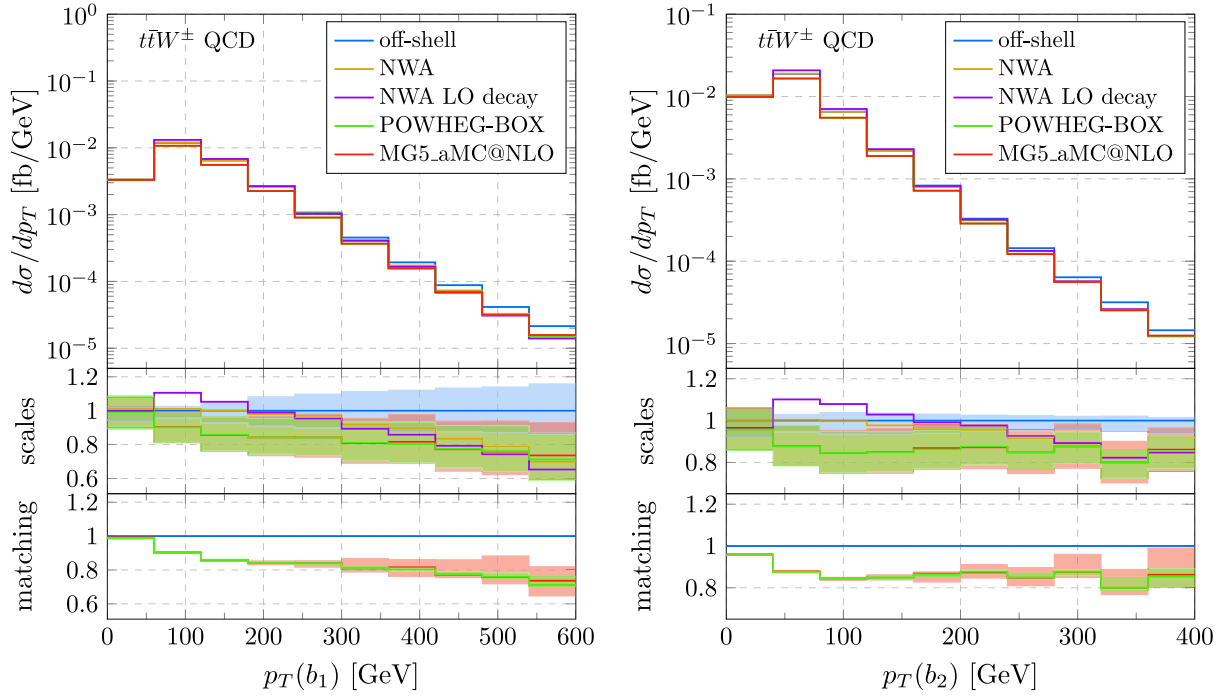
FIG. 2. Differential cross section distribution in the $3\ell$ fiducial region as a function of the transverse momentum of the hardest (lhs) and the second hardest (rhs) $b$ jet for the $pp \to t\bar{t}W^{\pm}$ QCD process. The uncertainty bands correspond to independent variations of the renormalization and factorization scales (middle panel) and of the matching parameters (bottom panel).

obtained using the central values of both scale and matching parameters) for the various predictions employed in our study. The middle panel illustrates the scale uncertainty bands stemming from independent variations of factorization and renormalization scales. All curves are normalized to the central prediction of the off-shell calculation, and for ease of readability, we do not show uncertainty bands for the predictions based on the NWA. Finally, the bottom panel shows the matching uncertainties for the parton-shower-based predictions, which are estimated by a variation of the initial shower scale $\mu_Q$ in the case of MG5_aMC@NLO and of the various damping parameters in the case of the POWHEG-BOX.

On the left of Fig. 2, the transverse momentum distribution of the hardest $b$ jet is shown. We observe shape differences between the various predictions over the whole plotted range. Results in the full NWA have the same shape as those of the off-shell calculation for $p_T(b_1) \lesssim 300$ GeV. However, all of them differ by 27%–35% from the full calculation at $p_T \sim 600$ GeV. This is not surprising since in this region the single-resonant contribution from $pp \to tWWb$ becomes sizable.[3] These kinds of corrections can only be provided by an off-shell computation, and the comparison cannot be improved by including, among

others, NNLO QCD corrections in the NWA for the $t\bar{t}W^{\pm}$ process or by incorporating multijet merging. The dominant uncertainties for all predictions are attributed to missing higher-order corrections. In the case of the full off-shell calculation, the scale sensitivity is the smallest, starting from ±5% and increasing up to ±15% toward the end of the plotted spectrum. On the contrary, the scale uncertainties of parton-shower-based results already start at 10% and grow up to 21%–26% at high $p_T$. Matching uncertainties, on the other hand, are negligible below 300 GeV but increase up to ±7% in the case of the POWHEG-BOX and ±12% for MG5_aMC@NLO at higher $p_T$.

For the transverse-momentum distribution of the second hardest $b$ jet, displayed on the right-hand side of Fig. 2, the situation changes slightly. While the general shape of the full NWA prediction diverges from the off-shell result above $p_T \geq 120$ GeV, we observe that the shapes of the POWHEG-BOX and MG5_aMC@NLO spectra above 80 GeV are nearly identical with the off-shell result over the whole plotted range up to an overall shift in the normalization by −15%. Remarkably, the scale uncertainties of the off-shell calculation are rather constant and below 6%. Comparing this to the corresponding 15% uncertainties for $p_T(b_1)$ indicates that $p_T(b_2)$ is less sensitive to new LO-like contributions in the real radiation part. Also for the POWHEG-BOX and MG5_aMC@NLO results, the scale uncertainties are constant and of the order of ±10%. As for the case of the hardest $b$ jet, matching uncertainties become comparable in size only in the tail of the distribution.

---
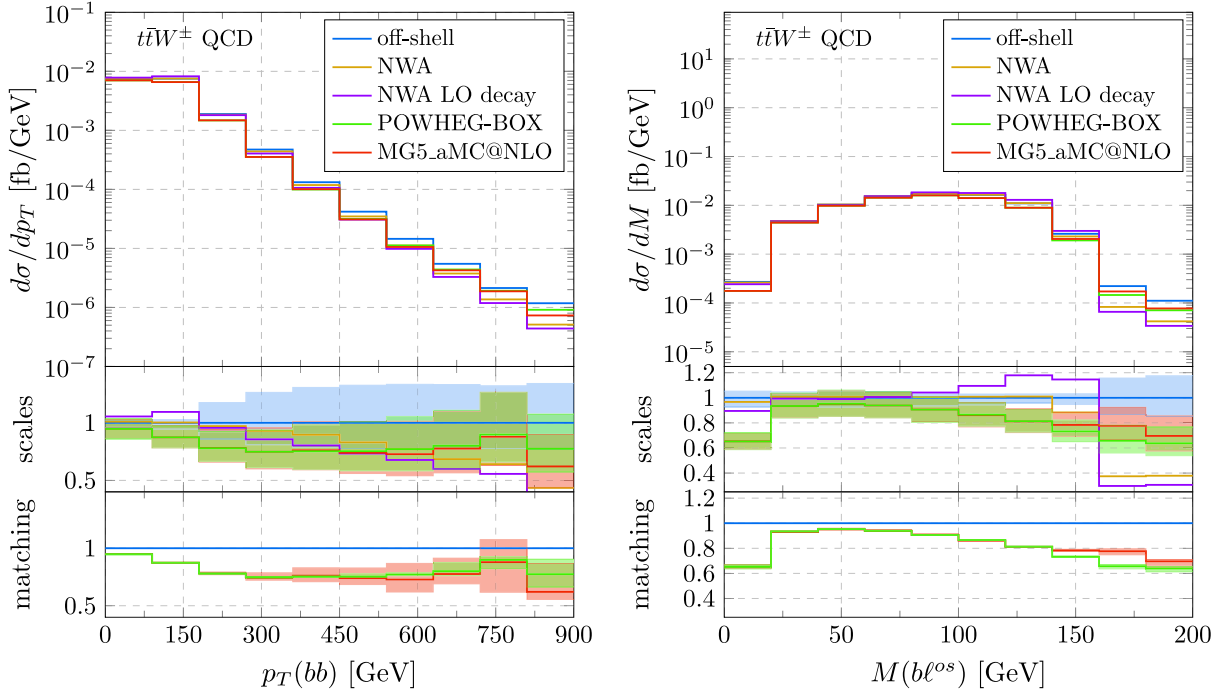
[3]We checked this explicitly via a LO computation for $pp \to tWWb$ that removes all double-resonant diagrams. Even though this approach is not gauge invariant, it provides a qualitative explanation.

FIG. 3.   Differential cross section distribution in the $3\ell$ fiducial region as a function of the transverse momentum of the system of the two hardest $b$ jets (lhs) and the minimal invariant mass of a $b$ jet and the opposite-sign lepton $\ell^{os}$ (rhs) for the $pp \to t\bar{t}W^{\pm}$ QCD process. The uncertainty bands correspond to independent variations of the renormalization and factorization scales (middle panel) and of the matching parameters (bottom panel).

For the transverse momentum of the system of the two hardest $b$ jets shown on the left-hand side of Fig. 3, we observe first of all the enlarged uncertainty band, of the order of $\pm 30\%$, for the off-shell calculation, which indicates that the observable is very sensitive to extra jet radiation. Again starting from $p_T \sim 300$ GeV, the NWA increasingly deviates from the off-shell calculation all the way up to 55% at the end of the spectrum. This can be understood from the fact that in the tail of the distribution the single-resonant contribution for $pp \to tWWb$ scattering, which is only included in the full off-shell computation, becomes quite large. On the other hand, the parton-shower-based predictions lie somewhat in between the NWA and the off-shell calculation for $p_T \gtrsim 600$ GeV. Within the estimated uncertainties, the parton-shower results are fully compatible with the full off-shell calculation over the whole considered range.

On the right of Fig. 3, we show the invariant mass of the opposite-sign lepton $\ell^{os}$ and the $b$ jet that minimizes the invariant mass itself. This observable is especially sensitive to off-shell effects and additional radiation since it has a natural kinematical edge at $M(b\ell^{os}) \leq \sqrt{m_t^2 - m_W^2} \approx 152$ GeV in the case of the $t \to W^+ b$ on-shell decay. Thus, this observable is indeed particularly interesting for top-quark mass measurements [82–85]. The full NWA recovers the shape of the off-shell result for $M(b\ell^{os}) \leq 140$ GeV but deviates up to 60% in the tail of the distribution. If top-quark decays are treated at

leading-order accuracy in the NWA also, the kinematical boundary is not described well, even below the edge. Finally, the parton-shower-based predictions that account for multiple emissions in the top-quark decays wash out the kinematic edge even further. A considerable fraction of events is pushed above the edge and populates the tail of the distribution. We find only a difference of the order of 30% with respect to the off-shell calculation. However, here as well, the tail of the distribution receives sizable contributions from the single-resonant $tWWb$ scattering. Scale uncertainties for the off-shell calculation are of the order of $\pm 5\%$ below the kinematic edge and $\pm 15\%$ above. On the other hand, the POWHEG-BOX and MG5_aMC@NLO obtain roughly $\pm 10\%$ below and $\pm 20\%$ uncertainties above the edge, while matching uncertainties are negligible throughout the whole range.

Next, we discuss the transverse momentum of the opposite-sign lepton $\ell^{os}$ and the $H_T^{\text{lep}}$ observable, which is defined as

$$H_T^{\text{lep}} = \sum_{i=1}^{3} p_T(\ell_i). \tag{27}$$

Both observables are shown in Fig. 4. In the case of the transverse momentum distribution, we note that the full NWA gives an equivalent description compared to the off-shell prediction of the observable over the whole plotted
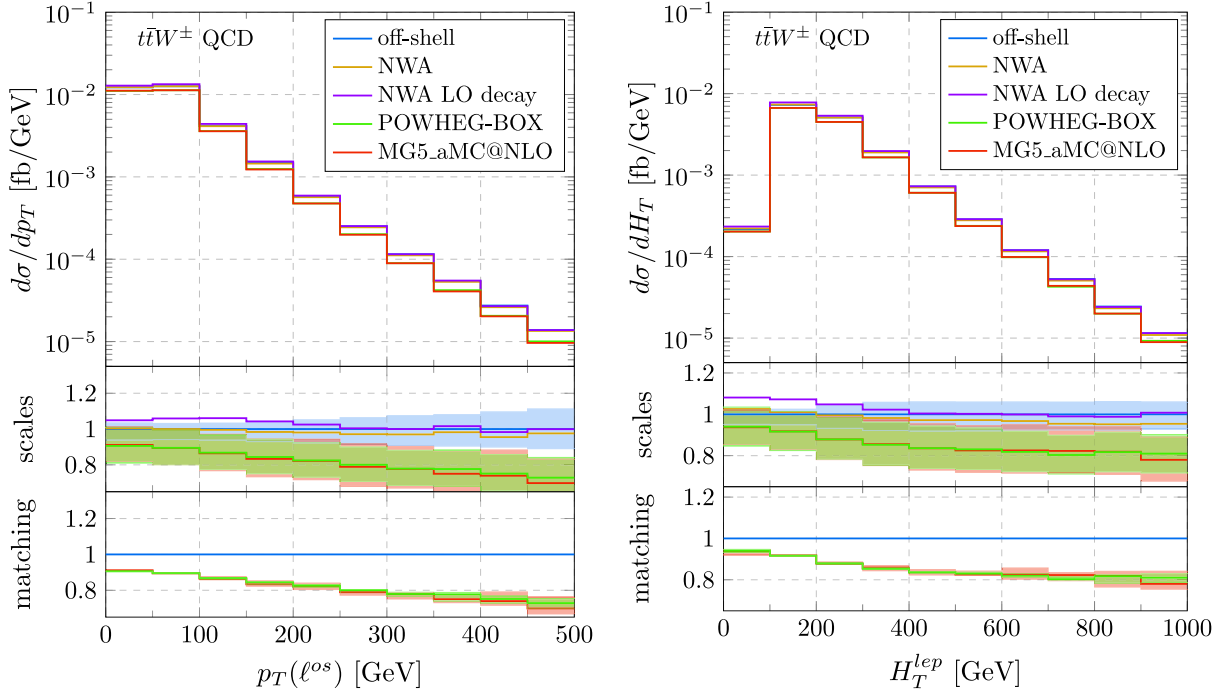
FIG. 4.    Differential cross section distribution in the $3\ell$ fiducial region as a function of the transverse momentum of the opposite-sign lepton $\ell^{os}$ (lhs) and the $H_T^{\text{lep}}$ observable (rhs) for the $pp \to t\bar{t}W^{\pm}$ QCD process. The uncertainty bands correspond to independent variations of the renormalization and factorization scales (middle panel) and of the matching parameters (bottom panel).

range. If NLO QCD corrections to the top-quark decays are ignored, then the prediction at the beginning of the spectrum with $p_T \leq 200$ GeV overshoots the off-shell results mildly by $+6\%$. The tail of the distribution is again in excellent agreement with the off-shell calculation. On the contrary, the parton-shower matched predictions obtain a very different shape compared to the fixed-order predictions. Starting from a difference of about $-10\%$, the parton-shower predictions diverge further up to $-30\%$ at the end of the plotted range. In addition, the scale uncertainties of the off-shell result are below 11%, while they are at most 15% for the POWHEG-BOX and 20% for MG5_aMC@NLO. Thus, starting from $p_T \geq 350$ GeV, the uncertainty bands do not overlap anymore. In comparison, matching uncertainties are negligible in the considered range.

For the $H_T^{\text{lep}}$ observable on the right of Fig. 4, we observe a similar trend. Even though predictions based on the full NWA have minor shape differences, they are fully compatible with the off-shell calculation within the uncertainties. For the off-shell results, the scale uncertainties are estimated to be below 8% in the whole plotted range. The POWHEG-BOX and MG5_aMC@NLO predictions are hardly distinguishable and show a different shape, with deviations of up to 20% in the tail of the distribution, when compared to the off-shell results. Only because of the larger scale uncertainty of the parton-shower matched predictions, which are of the order of 15%, the curves are compatible with the off-shell prediction up to 700 GeV. Above that point, the uncertainty bands do not overlap anymore.

## B. Electroweak production of $t\bar{t}W^{\pm}$

Let us now turn to the discussion of the electroweak production of the $pp \to t\bar{t}W^{\pm}$ process including decays at $\mathcal{O}(\alpha_s\alpha^8)$. We start again by investigating the integrated fiducial cross sections and turn to differential distributions afterward.

### 1. Integrated fiducial cross sections

In the case of the full off-shell computation, the integrated fiducial cross section evaluates to

$$\sigma_{\text{off-shell}}^{\text{NLO}} = 0.206_{-0.034(17\%)}^{+0.045(22\%)} \text{ fb.} \tag{28}$$

We observe large scale uncertainties of the order of $\pm 20\%$ at NLO, which reflects the fact that the $\alpha_s$ dependence only starts at NLO. For the EW part, the NLO QCD corrections are anomalously large and of the order of $\mathcal{K} = \text{NLO}/\text{LO} \approx 18$, due to the $t$-channel $tW \to tW$ scattering in the $qg$ channels that opens up at NLO. Overall, the EW contribution amounts to 13% of the dominant NLO QCD contributions to $t\bar{t}W^{\pm}$ production, i.e.,

$$\left(\frac{\sigma_{\text{QCD}}^{\text{NLO}} + \sigma_{\text{EW}}^{\text{NLO}}}{\sigma_{\text{QCD}}^{\text{NLO}}}\right)_{\text{off-shell}} = 1.13. \tag{29}$$

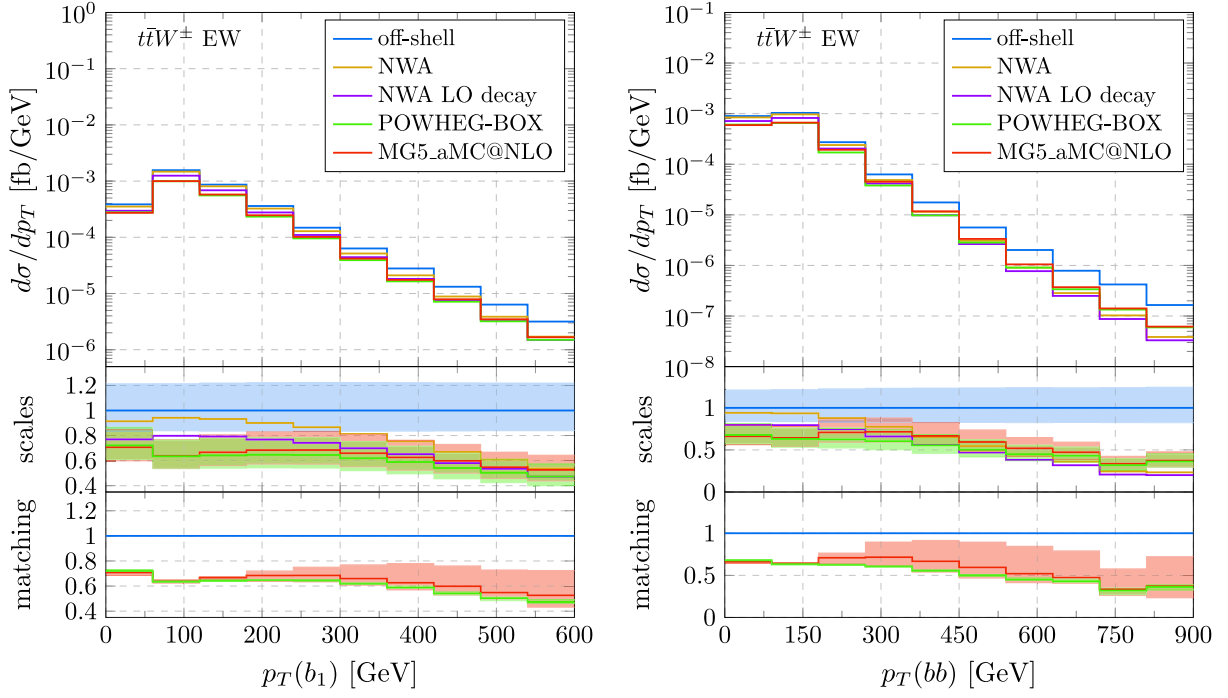If instead the NWA is employed, we find the following cross sections:

FIG. 5.   Differential cross section distribution in the $3\ell$ fiducial region as a function of the transverse momentum of the hardest $b$ jet (lhs) and of the system of the two hardest $b$ jets (rhs) for the $pp \to t\bar{t}W^{\pm}$ EW process. The uncertainty bands correspond to independent variations of the renormalization and factorization scales (middle panel) and of the matching parameters (bottom panel).

$$\sigma_{\text{NWA}}^{\text{NLO}} = 0.190^{+0.041(22\%)}_{-0.031(16\%)} \text{ fb},$$

$$\sigma_{\text{NWA LOdec}}^{\text{NLO}} = 0.162^{+0.035(22\%)}_{-0.026(16\%)} \text{ fb}. \tag{30}$$

First of all, we notice that NLO QCD corrections to top-quark decays increase the cross section by 17% but do not affect the overall scale uncertainties, which are of the same order as in the case of the full off-shell calculation. Furthermore, besides the large corrections from the top-quark decays, we also observe large off-shell effects of the order of 8% at the level of integrated cross sections. Such effects originate from $WW \to WW$ scattering contributions as we have checked explicitly at LO where the off-shell effects are even larger and of the order of 12%.

Finally, the obtained cross sections via parton-shower matched calculations are given by

$$\sigma_{\text{PWG}}^{\text{NLO+PS}} = 0.133^{+0.028(21\%)}_{-0.021(16\%)} \text{ fb},$$

$$\sigma_{\text{MG5}}^{\text{NLO+PS}} = 0.136^{+0.028(21\%)}_{-0.022(16\%)} \text{ fb}. \tag{31}$$

The event generators have the smallest cross section among all the approaches considered in our study. The parton-shower matched results predict a 34%–35% smaller cross section if compared to the full off-shell result. Also in the case of the EW contribution, the POWHEG-BOX and MG5_aMC@NLO results align very well and are 16%–18% smaller than the predictions obtained with the NWA with

LO top-quark decays. This is the same level of reduction of the cross section as observed in the QCD contribution and, as in that case, can be attributed to additional radiation in top decays. However, in the EW case, parton-shower-based results show the same level of uncertainties as all the other approaches.

### 2. Differential distributions

Let us now turn again to the differential comparison of the various computational approaches in our study.

First, we focus on $b$-jet observables like the transverse momentum of the hardest $b$ jet and the pair of the two hardest $b$ jets, as shown in Fig. 5. It is evident that, even though the scale uncertainties of the full off-shell prediction are of the order of $\pm 20\%$, none of the other predictions can reproduce the shape of the spectrum. While the full NWA at least agrees with the off-shell prediction for low transverse momenta $p_T \lesssim 200$ GeV within scale uncertainties, the other predictions differ by 20%–40% already in the bulk of the distribution. Toward the end of the plotted spectrum, all predictions deviate by 50% from the full off-shell calculation. Missing higher-order corrections are the dominant source of uncertainties. However, while matching uncertainties stay below 5% for the POWHEG-BOX they can increase up to 20%–40% for MG5_aMC@NLO. For the transverse momentum of the system of the two hardest $b$ jets shown on the right-hand side of Fig. 5, we observe even stronger deviations. As in the case of the QCD production
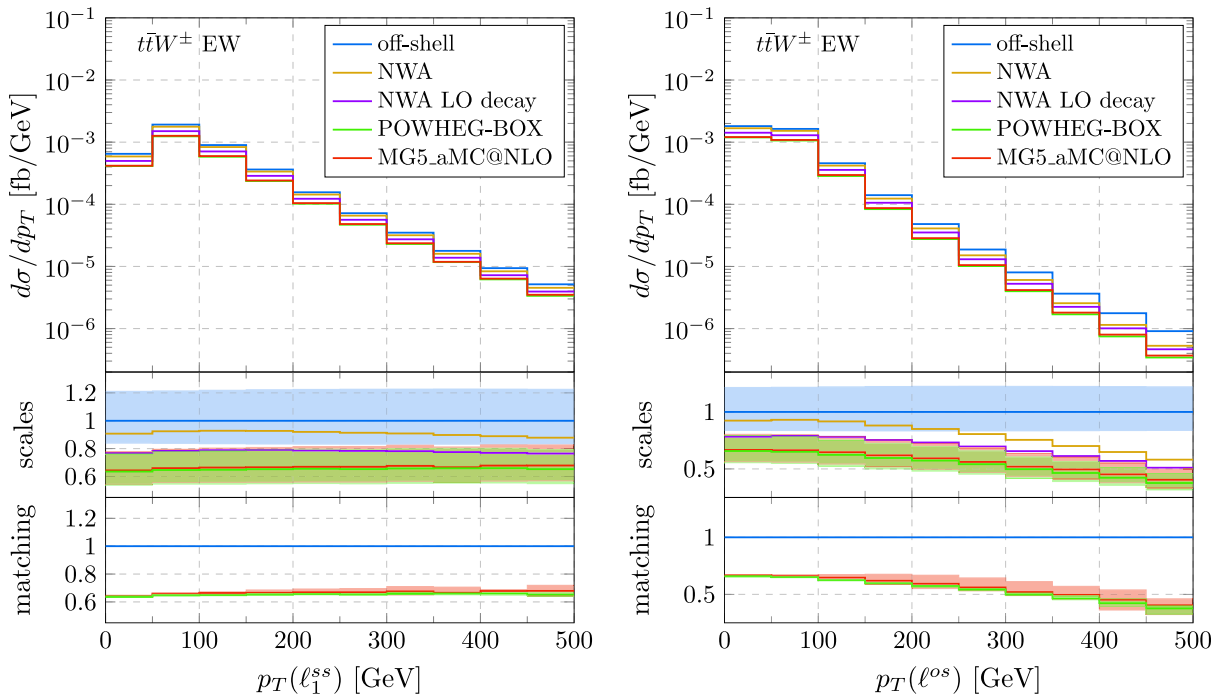
FIG. 6.    Differential cross section distribution in the $3\ell$ fiducial region as a function of the transverse momentum of the hardest same-sign lepton $\ell_1^{ss}$ (lhs) and the opposite-sign lepton $\ell^{os}$ (rhs) for the $pp \to t\bar{t}W^{\pm}$ EW process. The uncertainty bands correspond to independent variations of the renormalization and factorization scales (middle panel) and of the matching parameters (bottom panel).

mode, the scale uncertainties for this observable are slightly larger and of the order of 20%–25%. Nonetheless, all predictions diverge from the off-shell result by 65%–75% at $p_T \approx 900$ GeV. The estimated matching uncertainties are very different between the POWHEG-BOX and MG5_aMC@NLO. While the parton-shower starting scale $\mu_Q$ has a big impact for MG5_aMC@NLO and can affect the shape the distribution by up to 90%, the dependence of the various damping parameters in the POWHEG-BOX induces differences up to $\pm10\%$.

Next, we investigate lepton observables such as the transverse momentum of the hardest same-sign lepton $\ell_1^{ss}$ and the opposite-sign lepton $\ell^{os}$ as depicted in Fig. 6. These two observables behave very differently. In the case of $p_T(\ell_1^{ss})$, the lepton can either originate from the top-quark decay or from the $W$ boson radiated in the initial state. For the off-shell calculation, even more topologies are possible, as single- and nonresonant contributions are present. However, we find that all predictions generate a very similar shape of the spectrum and differences are mainly due to overall normalizations. To be precise, the full NWA is globally 10%, the NWA with LO decays is 20%, and the parton-shower predictions are 35% lower than the full off-shell calculation. Scale uncertainties are for all predictions at the level of $\pm20\%$. However, because of the overall shift in the normalization, the parton-shower results barely overlap with the full off-shell results. In addition, matching uncertainties are negligible for both parton-shower predictions. On the other hand, when we look at

the transverse momentum of the opposite-sign lepton $\ell^{os}$, we expect larger off-shell effects. This is due to fact that, in the case of the double-resonant $t\bar{t}W^{\pm}$ contribution, the lepton can only originate from a top-quark decay, which is not the case for the full off-shell computation. Indeed, we find that all approximations undershoot the tail of the distribution by 40%–60%. Comparing the same observable to the QCD production mode as shown in Fig. 4, we notice that the single-resonant contribution must be much larger in the EW contribution. As in the previous cases, the residual dependence on the renormalization and factorization scales are the dominant uncertainties, which for all predictions are of the order of 22%. Nonetheless, the matching uncertainties become sizable in the tail of the spectrum and can reach up to 13% for the POWHEG-BOX and 20% for MG5_aMC@NLO.

At last, we discuss the transverse momentum and the rapidity of the leading light jet as shown in Fig. 7. First of all, we notice that for both observables the NWA reproduces the shape of the full off-shell prediction perfectly. The curves only differ by an overall shift of −10% in the normalization. Additionally, we can infer that NLO QCD corrections to the decay are not important for this observable and that both the full NWA and NWA with LO decays are compatible with the full off-shell prediction within the scale dependence. On the other hand, the parton-shower matched calculations receive large corrections. Especially in the beginning of the transverse momentum, spectrum deviations up to 85% are visible. The uncertainties of the various predictions turn out to be very different. However,
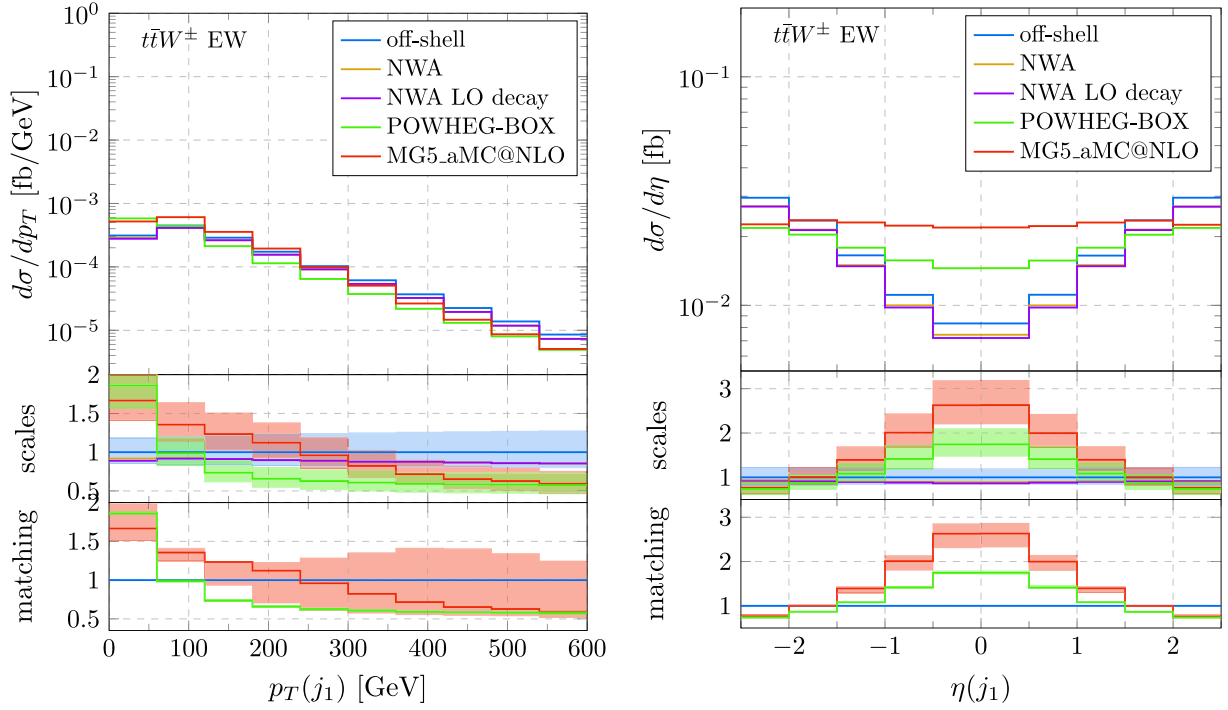
FIG. 7. Differential cross section distribution in the $3\ell$ fiducial region as a function of the transverse momentum (lhs) and the pseudorapidity (rhs) of the leading light jet for the $pp \to t\bar{t}W^{\pm}$ EW process. The uncertainty bands correspond to independent variations of the renormalization and factorization scales (middle panel) and of the matching parameters (bottom panel).

the full off-shell calculation has a residual scale dependence at the level of 20%–25%, which is at the same level as for the parton-shower-based computations. In addition, in the POWHEG-BOX, the spectrum is very stable with respect to the various matching parameters with shape modifications below 4%. Thus, in the case of the POWHEG-BOX, the dominant uncertainties are attributed to missing higher-order corrections. On the contrary, the MG5_aMC@NLO curve depends crucially on the choice of the initial shower scale $\mu_Q$ and can alter the tails of the distribution by more than 100%, making the matching uncertainties the dominant source of uncertainties. For the rapidity of the hardest light jet, shown on the right of Fig. 7, we also find large parton-shower corrections. While the leading jet in fixed-order perturbation theory is constrained to the very forward region, the inclusion of additional radiation in the parton-shower evolution fills the gap in the central rapidity region. Thus, parton-shower matched calculations predict significantly more events in the central regions with nearly 200% corrections. Still, the POWHEG-BOX and MG5_aMC@NLO predictions are very different. Similar effects for these two observables have been already observed in Ref. [36] in the case of an on-shell $t\bar{t}W^{\pm}$ signature.

## V. COMBINED QCD AND ELECTROWEAK PRODUCTION OF $t\bar{t}W^{\pm}$

In the following, we provide combined results including the QCD and EW production modes discussed in Sec. IV

and propose a way to improve theoretical predictions in the absence of fully exclusive NLO parton-shower event generators based on full off-shell $pp \to \ell^+\nu\ell^-\nu\ell^{\pm}\nu b\bar{b}$ matrix elements.

In the previous sections, we have seen that the theoretical predictions with parton-shower effects include many kinematical features that are not accessible to a fixed-order NLO computation. However, while comparing the various approaches to the full off-shell computation, we observed that the single-resonant contributions start to dominate in some phase-space regions and give rise to sizable corrections in the tail of dimensionful observables. Naturally, the question arises as to how one can combine these two different theoretical predictions that describe the same observables but differ in the amount and kind of physical effects taken into account. In the case at hand, we would like to supplement a NLO parton-shower matched computation with full off-shell effects. Our method of choice is the additive combination

$$\frac{d\sigma^{\text{th}}}{dX} = \frac{d\sigma^{\text{NLO+PS}}}{dX} + \frac{d\Delta\sigma_{\text{off-shell}}}{dX}, \quad \text{with}$$

$$\frac{d\Delta\sigma_{\text{off-shell}}}{dX} = \frac{d\sigma^{\text{NLO}}_{\text{off-shell}}}{dX} - \frac{d\sigma^{\text{NLO}}_{\text{NWA}}}{dX}, \tag{32}$$

where fixed-order full off-shell effects are simply added to a parton-shower based computation. Let us comment on the choice of subtraction used in defining the $d\Delta\sigma_{\text{off-shell}}/dX$

TABLE I.   Integrated fiducial cross sections for the $pp \to t\bar{t}W^{\pm}$ process for various approaches. We use the POWHEG-BOX to obtain the NLOPS results.

| Type | QCD (fb) | EW (fb) | QCD + EW (fb) | (QCD + EW)/QCD |
|---|---|---|---|---|
| Full off-shell | $1.58^{+0.05(3\%)}_{-0.10(6\%)}$ | $0.206^{+0.045(22\%)}_{-0.034(16\%)}$ | $1.79^{+0.10(6\%)}_{-0.13(7\%)}$ | 1.13 |
| NLOPS | $1.40^{+0.16(11\%)}_{-0.15(11\%)}$ | $0.133^{+0.028(21\%)}_{-0.021(16\%)}$ | $1.53^{+0.19(12\%)}_{-0.17(11\%)}$ | 1.10 |
| NLOPS + $\Delta\sigma$ | $1.41^{+0.16(11\%)}_{-0.16(11\%)}$ | $0.149^{+0.028(19\%)}_{-0.028(19\%)}$ | $1.56^{+0.21(13\%)}_{-0.21(13\%)}$ | 1.11 |

contribution. The subtraction of the full NWA removes approximately the double-counting between the double-resonant contributions in the full off-shell and the NLO + PS computation. Strictly speaking, one should subtract the NLO + PS result expanded to the same order in $\alpha_s$ as the full off-shell computation. This would include parton-shower specific contributions due to parton-shower radiation in the top-quark decays. We approximate this additional parton-shower radiation by subtracting the full NWA with NLO top-quark decays instead. We note that our differential corrections $d\Delta\sigma_{\text{off-shell}}/dX$ are independent of the parton-shower event generator employed. In addition, $d\Delta\sigma_{\text{off-shell}}/dX$ provides differential corrections for the single- and nonresonant contributions as well as interference effects in an approximate way. To estimate the theoretical uncertainty of our improved predictions, we compute the scale variations and matching uncertainties independently and combine them by adding them in quadrature,

$$\delta^{\text{th}} = \sqrt{(\delta^{\text{NLO+PS}}_{\text{scale}})^2 + (\delta^{\text{NLO+PS}}_{\text{matching}})^2 + (\delta^{\Delta\sigma}_{\text{scale}})^2}, \quad (33)$$

where $\delta^{\Delta\sigma}_{\text{scale}}$ is the estimated uncertainty of $d\Delta\sigma_{\text{off-shell}}/dX$ and computed from correlated scale variations. Finally, all contributions to $\delta^{\text{th}}$ are symmetrized.

Finally, given the good agreement we found between the POWHEG-BOX and MG5_aMC@NLO in the course of our study, and considering the independence of the $d\Delta\sigma_{\text{off-shell}}/dX$ of the parton shower used, we will show in the following results for the POWHEG-BOX only. Incidentally, if theoretical predictions including multijet merging are available, then the aforementioned differential corrections can also be included.

### A. Integrated fiducial cross sections

In Table I, we present results for the integrated fiducial cross section.

We observe that for the combined QCD + EW result including the $\Delta\sigma$ correction increases the NLOPS cross section by 2%. On the other hand, looking at the individual QCD and EW contributions, one can notice that the impact of $\Delta\sigma$ on the EW part is much larger and of the order of 12%, while for the QCD part, it is about 1%.

Let us note that the full off-shell effects increase the relative contribution due to the electroweak production process by 3% with respect to the NLOPS prediction.

### B. Differential distributions

Turning to differential distributions, we can now investigate how well our improved NLOPS + $\Delta\sigma$ predictions capture off-shell effects in an approximate way. We show our results as plots with three panels: the upper panel shows the central predictions, the middle one shows the ratio to the full off-shell prediction, while the bottom one shows for each prediction the impact of the electroweak contribution over the pure QCD result. Also shown in the middle panel are uncertainty bands for the full off-shell and the NLOPS calculation, as well as total uncertainties for the NLOPS + $\Delta\sigma$ results that are obtained according to Eq. (33).

Starting with the transverse momentum of the hardest $b$ jet shown on the left of Fig. 8, we observe that in the bulk of the distribution up to 250 GeV the corrections due to the approximate off-shell effects are small and the result is dominated by parton-shower effects. However, the tails of the distribution receive sizable corrections due to $d\Delta\sigma_{\text{off-shell}}/dX$ with respect to the NLOPS result. Specifically, they amount to +48% at the end of the plotted spectrum. As parton-shower corrections in the tails are small, the NLOPS + $\Delta\sigma$ predictions agree well within the estimated uncertainties with the off-shell computation in this region. Furthermore, we can infer from the bottom panel of the plot that the EW contribution behaves differently in the off-shell computation than in the NLOPS prediction. In the latter case, the EW contribution is a very flat +10% correction on top of the dominant QCD contribution. If the full off-shell calculation is employed, a clear trend is visible. At the beginning of the spectrum, the EW channels contribute a +11% correction that steadily grows to +15% in the tails of the distribution. Our theoretical NLOPS + $\Delta\sigma$ prediction clearly captures the large off-shell corrections in the tails. The situation is qualitatively different if we consider the transverse momentum of the system of the two hardest $b$ jets depicted on the right of Fig. 8. Here, the improved NLOPS + $\Delta\sigma$ prediction overshoots the off-shell tails by 30%. The reason for this is that the tails of the distribution receive large corrections from single-resonant top-quark contributions but also from parton-shower radiation. The theoretical uncertainties are estimated to be of the order of 20%. As in the previous case, we observe
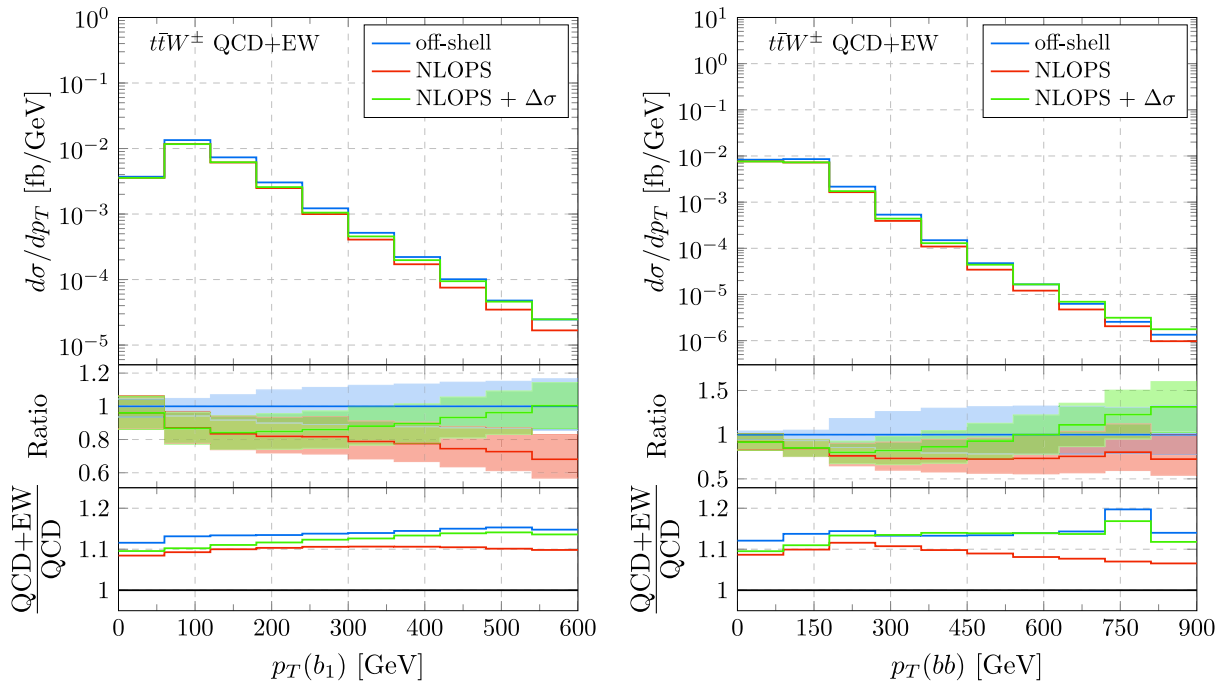
FIG. 8.    Differential cross section distribution in the $3\ell$ fiducial region as a function of the transverse momentum of the hardest $b$ jet (lhs) and of the system of the two hardest $b$ jets (rhs) for the $pp \to t\bar{t}W^{\pm}$ QCD + EW process. The uncertainty bands correspond to scale variations (off-shell) and total uncertainties (NLOPS) (middle panel). The differential impact of the EW contribution is shown as well (bottom panel).
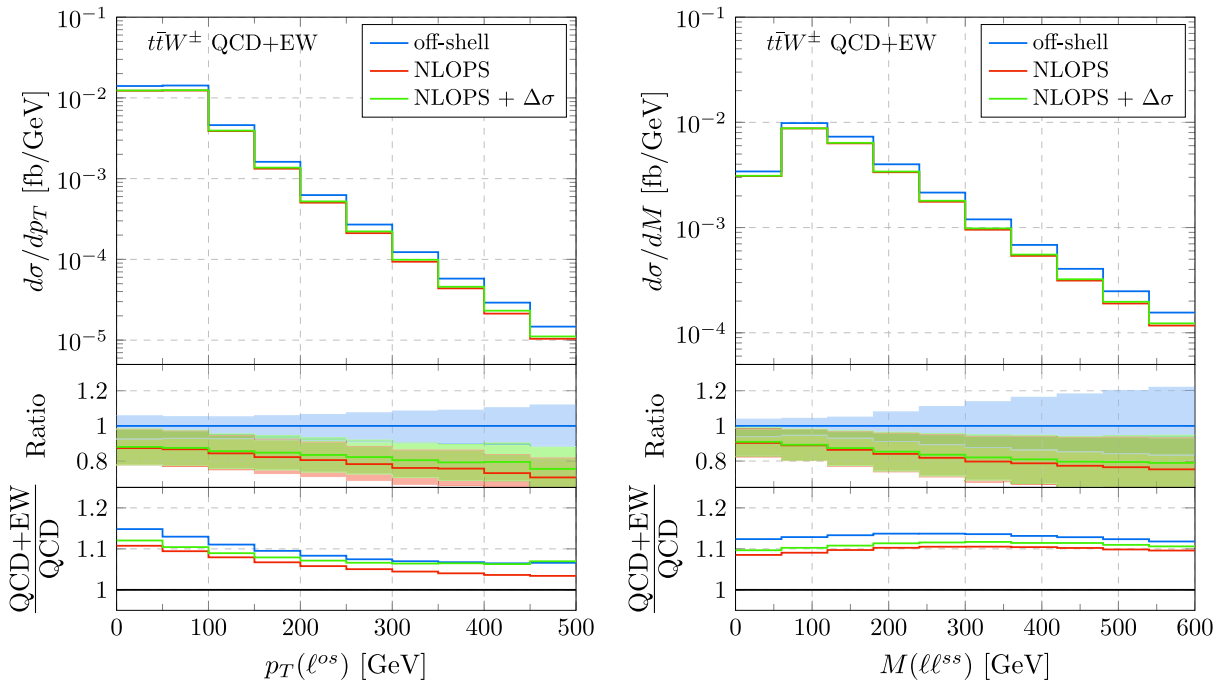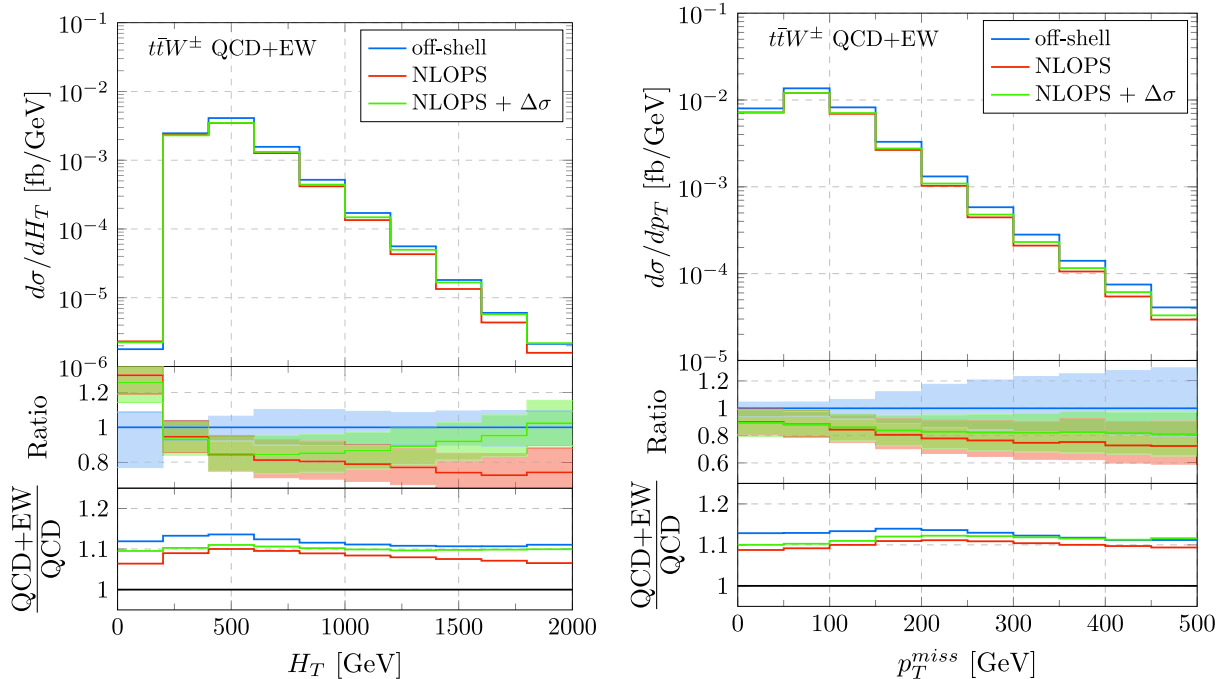


FIG. 9.    Differential cross section distribution in the $3\ell$ fiducial region as a function of the transverse momentum of the opposite-sign lepton $\ell^{os}$ (lhs) and the invariant mass of the same-sign lepton pair (rhs) for the $pp \to t\bar{t}W^{\pm}$ QCD + EW process. The uncertainty bands correspond to scale variations (off-shell) and total uncertainties (NLOPS) (middle panel). The differential impact of the EW contribution is shown as well (bottom panel).

FIG. 10. Differential cross section distribution in the $3\ell$ fiducial region as a function of the total transverse momentum $H_T$ (lhs) and the missing transverse momentum (rhs) for the $pp \to t\bar{t}W^{\pm}$ QCD + EW process. The uncertainty bands correspond to scale variations (off-shell) and total uncertainties (NLOPS) (middle panel). The differential impact of the EW contribution is shown as well (bottom panel).

that the EW contribution behaves qualitatively differently in the full off-shell calculation. In the NLOPS computation, the impact of the EW production mode peaks around $p_T \sim 225$ GeV and decreases slowly for larger transverse momenta. On the contrary, for the full off-shell calculation, the EW contribution is a flat $+15\%$ correction above $p_T \gtrsim 150$ GeV.

Turning now to lepton observables, we show the transverse momentum of the opposite-sign lepton $\ell^{os}$ on the left and the invariant mass of the same-sign lepton pair on the right of Fig. 9. Contrary to the $b$-jet observables, we only find minor corrections of at most $+8\%$ over the NLOPS results. This is expected since for the dominant QCD contribution the results based on the NWA and the full off-shell calculation are in very good agreement. For the spectrum of the transverse momentum distribution, the EW contributions contribute $10\%$–$15\%$, depending on the computational approach employed, at the beginning of the spectrum, while they decrease to $3\%$–$7\%$ at the end of the spectrum. For the invariant mass spectrum of the same-sign lepton pair, the EW channels contribute a rather constant $10\%$–$12\%$ correction over the whole spectrum. In this case, we do not observe sizable improvements when NLOPS $+ \Delta\sigma$ is used instead of NLOPS.

At last, we study the differential distributions of the $H_T$ observable and $p_T^{\mathrm{miss}}$ as shown in Fig. 10. Let us remind the reader that the $H_T$ observable is defined as

$$H_T = \sum_{i=1}^{3} p_T(\ell_i) + \sum_{i=1}^{2} p_T(b_i) + p_T^{\mathrm{miss}}, \quad (34)$$

where only the two hardest $b$ jets are included. For the $H_T$ observable shown on the left of Fig. 10, we observe that the NLOPS $+ \Delta\sigma$ predictions are in better agreement with the off-shell calculation. While the bulk of the distribution is dominated by parton-shower effects, the tail receives large single-resonant contributions of the order of $40\%$. As in all previous cases, the full off-shell result obtains slightly larger EW contributions than in the case of NLOPS predictions. On the other hand, the $p_T^{\mathrm{miss}}$ observable only shows small corrections from single- and nonresonant contributions below $12\%$. The NLOPS $+ \Delta\sigma$ prediction is fully compatible with the original NLOPS result within the estimated uncertainties. For the pure NLOPS prediction, the EW production mode provides a nearly constant correction of $10\%$, while in the case of the full off-shell result, the corrections are slightly larger with $+14\%$ at the beginning of the distribution.

## VI. CONCLUSIONS

In this work, we consider various approaches to the theoretical computation of QCD and EW production of multilepton final states for the $pp \to t\bar{t}W^{\pm}$ processes and study the impact of modeling differences in the light of

recent tensions between Standard Model theoretical predictions and experimental measurements.

NLOPS event generators and full off-shell fixed-order calculations lend themselves better to describing different fiducial regions of phase space. For instance, for dimensionful observables such as invariant masses and transverse momenta, we find large differences in the tails of distributions between the full off-shell calculation and any other approximate calculation based on on-shell top quarks. These off-shell contributions are dominantly attributed to single-resonant contributions that can only be included in an unambiguous way using the full off-shell calculation for the fully decayed final state. On the other hand, parton-shower effects impact the shape of various distributions over a broader range. In this paper, we propose a method to approximately combine the strengths of both approaches.

We also quantified for the first time the size of off-shell effects for the EW production process at $\mathcal{O}(\alpha_s \alpha^8)$ and found unusual large differences of the order of 8% already at the level of the integrated fiducial cross section. At the differential level, larger effects have been found as compared to the case of the QCD production mode at $\mathcal{O}(\alpha_s^3 \alpha^6)$.

In the absence of NLOPS theoretical predictions that comprise resonant-aware matched full off-shell calculations [86,87] for $t\bar{t}W^{\pm}$, we proposed in Sec. V improving on the current available predictions by combining NLOPS and full off-shell results in an additive way according to Eq. (32). Our proposal is an approximation that aims at removing the double-counting of double-resonant contributions between NLOPS and fixed-order computations but includes single- and nonresonant contributions at fixed order.

In this way, parton-shower effects can be retained, and off-shell corrections can be included in an approximate but event-generator-independent way for a large class of observables. We investigated in detail the impact of such improved theoretical predictions and provide conservative uncertainty estimates for the fully combined QCD + EW results. As we have observed in our study, the parton

shower evolution can have a sizable impact on differential distributions; therefore, in order to account for those shower effects also for the single- and nonresonant contributions, the proper matching of the full off-shell $t\bar{t}W^{\pm}$ calculation to parton showers is necessary.

Moving forward, we think that we could already learn a great deal by a detailed comparison of $t\bar{t}W^{\pm}$ unfolded data with the level of theoretical predictions presented in this paper. Beyond that, a fixed-order calculation of NNLO QCD corrections to the on-shell $t\bar{t}W^{\pm}$ process could help remove some of the theoretical uncertainty in both scale dependence and hard-radiation modeling. Equally important and equally challenging would be interfacing the full off-shell fixed-order calculation with parton-shower event generators.

## ACKNOWLEDGMENTS

[1] Georges Aad *et al.* (ATLAS Collaboration), Search for supersymmetry at $\sqrt{s} = 13$ TeV in final states with jets and two same-sign leptons or three leptons with the ATLAS detector, Eur. Phys. J. C **76**, 259 (2016).

[2] Vardan Khachatryan *et al.* (CMS Collaboration), Search for new physics in same-sign dilepton events in proton–proton collisions at $\sqrt{s} = 13$ TeV, Eur. Phys. J. C **76**, 439 (2016).

[3] Morad Aaboud *et al.* (ATLAS Collaboration), Search for supersymmetry in final states with two same-sign or three leptons and jets using 36 fb$^{-1}$ of $\sqrt{s} = 13$ TeV $pp$ collision data with the ATLAS detector, J. High Energy Phys. 09 (2017) 084; 08 (2019) 121(E).

[4] Albert M. Sirunyan *et al.* (CMS Collaboration), Search for physics beyond the standard model in events with two leptons of same sign, missing transverse momentum, and jets in proton–proton collisions at $\sqrt{s} = 13$ TeV, Eur. Phys. J. C **77**, 578 (2017).

[5] M. Aaboud *et al.* (ATLAS Collaboration), Observation of Higgs boson production in association with a top quark pair at the LHC with the ATLAS detector, Phys. Lett. B **784**, 173 (2018).

[6] Albert M. Sirunyan *et al.* (CMS Collaboration), Observation of t̄tH Production, Phys. Rev. Lett. **120**, 231801 (2018).

[7] ATLAS Collaboration, Analysis of $t\bar{t}H$ and $t\bar{t}W$ production in multilepton final states with the ATLAS detector, CERN Technical Report No. ATLAS-CONF-2019-045, 2019.

[8] CMS Collaboration, Higgs boson production in association with top quarks in final states with electrons, muons, and hadronically decaying tau leptons at $\sqrt{s} = 13$ TeV, CERN Report No. CMS-PAS-HIG-19-008, 2020.

[9] Morad Aaboud *et al.* (ATLAS Collaboration), Search for four-top-quark production in the single-lepton and opposite-sign dilepton final states in pp collisions at $\sqrt{s} = 13$ TeV with the ATLAS detector, Phys. Rev. D **99,** 052009 (2019).

[10] Albert M. Sirunyan *et al.* (CMS Collaboration), Search for production of four top quarks in final states with same-sign or multiple leptons in proton-proton collisions at $\sqrt{s} = 13$ TeV, Eur. Phys. J. C **80,** 75 (2020).

[11] Georges Aad *et al.* (ATLAS Collaboration), Evidence for $t\bar{t}t\bar{t}$ production in the multilepton final state in proton–proton collisions at $\sqrt{s} = 13$ TeV with the ATLAS detector, Eur. Phys. J. C **80,** 1085 (2020).

[12] Georges Aad *et al.* (ATLAS Collaboration), Measurement of the $t\bar{t}t\bar{t}$ production cross section in $pp$ collisions at $\sqrt{s} = 13$ TeV with the ATLAS detector, J. High Energy Phys. 11 (2021) 118.

[13] Georges Aad *et al.* (ATLAS Collaboration), Measurement of the $t\bar{t}W$ and $t\bar{t}Z$ production cross sections in pp collisions at $\sqrt{s} = 8$ TeV with the ATLAS detector, J. High Energy Phys. 11 (2015) 172.

[14] Vardan Khachatryan *et al.* (CMS Collaboration), Observation of top quark pairs produced in association with a vector boson in pp collisions at $\sqrt{s} = 8$ TeV, J. High Energy Phys. 01 (2016) 096.

[15] Morad Aaboud *et al.* (ATLAS Collaboration), Measurement of the $t\bar{t}Z$ and $t\bar{t}W$ production cross sections in multilepton final states using 3.2 fb$^{-1}$ of $pp$ collisions at $\sqrt{s} = 13$ TeV with the ATLAS detector, Eur. Phys. J. C **77,** 40 (2017).

[16] Albert M. Sirunyan *et al.* (CMS Collaboration), Measurement of the cross section for top quark pair production in association with a W or Z boson in proton-proton collisions at $\sqrt{s} = 13$ TeV, J. High Energy Phys. 08 (2018) 011.

[17] Morad Aaboud *et al.* (ATLAS Collaboration), Measurement of the $t\bar{t}Z$ and $t\bar{t}W$ cross sections in proton-proton collisions at $\sqrt{s} = 13$ TeV with the ATLAS detector, Phys. Rev. D **99,** 072009 (2019).

[18] Simon Badger, John M. Campbell, and R. K. Ellis, QCD corrections to the hadronic production of a heavy quark pair and a W-boson including decay correlations, J. High Energy Phys. 03 (2011) 027.

[19] John M. Campbell and R. Keith Ellis, $t\bar{t}W^{+-}$ production and decay at NLO, J. High Energy Phys. 07 (2012) 052.

[20] Jeff Asaf Dror, Marco Farina, Ennio Salvioni, and Javi Serra, Strong tW scattering at the LHC, J. High Energy Phys. 01 (2016) 071.

[21] S. Frixione, V. Hirschi, D. Pagani, H. S. Shao, and M. Zaro, Electroweak and QCD corrections to top-pair hadroproduction in association with heavy bosons, J. High Energy Phys. 06 (2015) 184.

[22] Rikkert Frederix, Davide Pagani, and Marco Zaro, Large NLO corrections in $t\bar{t}W^{\pm}$ and $t\bar{t}t\bar{t}$ hadroproduction from supposedly subleading EW contributions, J. High Energy Phys. 02 (2018) 031.

[23] Hai Tao Li, Chong Sheng Li, and Shi Ang Li, Renormalization group improved predictions for $t\bar{t}W^{\pm}$ production at hadron colliders, Phys. Rev. D **90,** 094009 (2014).

[24] Alessandro Broggio, Andrea Ferroglia, Giovanni Ossola, and Ben D. Pecjak, Associated production of a top pair and a W boson at next-to-next-to-leading logarithmic accuracy, J. High Energy Phys. 09 (2016) 089.

[25] Anna Kulesza, Leszek Motyka, Daniel Schwartländer, Tomasz Stebel, and Vincent Theeuwes, Associated production of a top quark pair with a heavy electroweak gauge boson at NLO + NNLL accuracy, Eur. Phys. J. C **79,** 249 (2019).

[26] Alessandro Broggio, Andrea Ferroglia, Rikkert Frederix, Davide Pagani, Benjamin D. Pecjak, and Ioannis Tsinikos, Top-quark pair hadroproduction in association with a heavy boson at NLO + NNLL including EW corrections, J. High Energy Phys. 08 (2019) 039.

[27] Anna Kulesza, Leszek Motyka, Daniel Schwartländer, Tomasz Stebel, and Vincent Theeuwes, Associated top quark pair production with a heavy boson: Differential cross sections at NLO + NNLL accuracy, Eur. Phys. J. C **80,** 428 (2020).

[28] Stefano Frixione and Bryan R. Webber, Matching NLO QCD computations and parton shower simulations, J. High Energy Phys. 06 (2002) 029.

[29] Stefano Frixione, Paolo Nason, and Bryan R. Webber, Matching NLO QCD and parton showers in heavy flavor production, J. High Energy Phys. 08 (2003) 007.

[30] F. Maltoni, M. L. Mangano, I. Tsinikos, and M. Zaro, Top-quark charge asymmetry and polarization in $t\bar{t}W^{\pm}$ production at the LHC, Phys. Lett. B **736,** 252 (2014).

[31] Fabio Maltoni, Davide Pagani, and Ioannis Tsinikos, Associated production of a top-quark pair with vector bosons at NLO in QCD: Impact on ttH searches at the LHC, J. High Energy Phys. 02 (2016) 113.

[32] Rikkert Frederix and Ioannis Tsinikos, Subleading EW corrections and spin-correlation effects in $t\bar{t}W$ multi-lepton signatures, Eur. Phys. J. C **80,** 803 (2020).

[33] Paolo Nason, A new method for combining NLO QCD with shower Monte Carlo algorithms, J. High Energy Phys. 11 (2004) 040.

[34] Stefano Frixione, Paolo Nason, and Carlo Oleari, Matching NLO QCD computations with Parton Shower simulations: The POWHEG method, J. High Energy Phys. 11 (2007) 070.

[35] M. V. Garzelli, A. Kardos, C. G. Papadopoulos, and Z. Trocsanyi, $t\bar{t}$ $W^{+-}$ and $t\bar{t}$ Z hadroproduction at NLO accuracy in QCD with Parton Shower and Hadronization effects, J. High Energy Phys. 11 (2012) 056.

[36] F. Febres Cordero, M. Kraus, and L. Reina, Top-quark pair production in association with a $W^{\pm}$ gauge boson in the POWHEG-BOX, Phys. Rev. D **103,** 094014 (2021).

[37] Stefan von Buddenbrock, Richard Ruiz, and Bruce Mellado, Anatomy of inclusive $t\bar{t}W$ production at hadron colliders, Phys. Lett. B **811,** 135964 (2020).

[38] ATLAS Collaboration, Modelling of rare top quark processes at $\sqrt{s} = 13$ TeV in ATLAS, CERN Report No. ATL-PHYS-PUB-2020-024, 2020.

[39] Rikkert Frederix and Ioannis Tsinikos, On improving NLO merging for $t\bar{t}W$ production, J. High Energy Phys. 11 (2021) 029.

[40] Giuseppe Bevilacqua, Huan-Yu Bi, Heribertus Bayu Hartanto, Manfred Kraus, and Malgorzata Worek, The simplest of them all: $t\bar{t}W^{\pm}$ at NLO accuracy in QCD, J. High Energy Phys. 08 (2020) 043.

[41] Ansgar Denner and Giovanni Pelliccioli, NLO QCD corrections to off-shell $t\bar{t}W^{+}$ production at the LHC, J. High Energy Phys. 11 (2020) 069.

[42] Giuseppe Bevilacqua, Huan-Yu Bi, Heribertus Bayu Hartanto, Manfred Kraus, Jasmina Nasufi, and Malgorzata Worek, NLO QCD corrections to off-shell $t\bar{t}W^{\pm}$ production at the LHC: Correlations and asymmetries, Eur. Phys. J. C **81,** 675 (2021).

[43] Ansgar Denner and Giovanni Pelliccioli, Combined NLO EW and QCD corrections to off-shell $t\bar{t}W$ production at the LHC, Eur. Phys. J. C **81,** 354 (2021).

[44] Richard D. Ball *et al.* (NNPDF Collaboration), Parton distributions from high-precision collider data, Eur. Phys. J. C **77,** 663 (2017).

[45] Andy Buckley, James Ferrando, Stephen Lloyd, Karl Nordström, Ben Page, Martin Rüfenacht, Marek Schönherr, and Graeme Watt, LHAPDF6: Parton density access in the LHC precision era, Eur. Phys. J. C **75,** 132 (2015).

[46] Ansgar Denner, S. Dittmaier, M. Roth, and D. Wackeroth, Electroweak radiative corrections to $e + e - - > WW - > 4$ fermions in double pole approximation: The RACOONWW approach, Nucl. Phys. **B587,** 67 (2000).

[47] G. Bevilacqua, M. Czakon, M. V. Garzelli, A. van Hameren, A. Kardos, C. G. Papadopoulos, R. Pittau, and M. Worek, HELAC-NLO, Comput. Phys. Commun. **184,** 986 (2013).

[48] Alessandro Cafarella, Costas G. Papadopoulos, and Malgorzata Worek, Helac-Phegas: A generator for all parton level processes, Comput. Phys. Commun. **180,** 1941 (2009).

[49] A. van Hameren, C. G. Papadopoulos, and R. Pittau, Automated one-loop calculations: A proof of concept, J. High Energy Phys. 09 (2009) 106.

[50] M. Czakon, C. G. Papadopoulos, and M. Worek, Polarizing the dipoles, J. High Energy Phys. 08 (2009) 085.

[51] Giovanni Ossola, Costas G. Papadopoulos, and Roberto Pittau, CutTools: A program implementing the OPP reduction method to compute one-loop amplitudes, J. High Energy Phys. 03 (2008) 042.

[52] G. Bevilacqua, M. Czakon, M. Kubocz, and M. Worek, Complete Nagy-Soper subtraction for next-to-leading order calculations in QCD, J. High Energy Phys. 10 (2013) 204.

[53] M. Czakon, H. B. Hartanto, M. Kraus, and M. Worek, Matching the Nagy-Soper parton shower at next-to-leading order, J. High Energy Phys. 06 (2015) 033.

[54] Ansgar Denner, S. Dittmaier, M. Roth, and D. Wackeroth, Predictions for all processes $e + e - - > 4$ fermions $+$gamma, Nucl. Phys. **B560,** 33 (1999).

[55] Ansgar Denner, S. Dittmaier, M. Roth, and L. H. Wieders, Electroweak corrections to charged-current $e + e - - > 4$ fermion processes: Technical details and further results, Nucl. Phys. **B724,** 247 (2005); **B854,** 504(E) (2012).

[56] M. Jezabek and Johann H. Kuhn, QCD corrections to semileptonic decays of heavy quarks, Nucl. Phys. **B314,** 1 (1989).

[57] K. G. Chetyrkin, R. Harlander, T. Seidensticker, and M. Steinhauser, Second order QCD corrections to Gamma(t—> W b), Phys. Rev. D **60,** 114015 (1999).

[58] Ansgar Denner, Stefan Dittmaier, Stefan Kallweit, and Stefano Pozzorini, NLO QCD corrections to off-shell top-antitop production with leptonic decays at hadron colliders, J. High Energy Phys. 10 (2012) 110.

[59] G. Bevilacqua, H. B. Hartanto, M. Kraus, T. Weber, and M. Worek, Off-shell vs on-shell modelling of top quarks in photon associated production, J. High Energy Phys. 03 (2020) 154.

[60] Steve Honeywell, Seth Quackenbush, Laura Reina, and Christian Reuschle, NLOX, a one-loop provider for Standard Model processes, Comput. Phys. Commun. **257,** 107284 (2020).

[61] Diogenes Figueroa, Seth Quackenbush, Laura Reina, and Christian Reuschle, Updates to the one-loop provider NLOX, Comput. Phys. Commun. **270,** 108150 (2022).

[62] Stefano Frixione, Eric Laenen, Patrick Motylinski, and Bryan R. Webber, Angular correlations of lepton pairs from vector boson and top quark decays in Monte Carlo simulations, J. High Energy Phys. 04 (2007) 081.

[63] J. Alwall, R. Frederix, S. Frixione, V. Hirschi, F. Maltoni, O. Mattelaer, H. S. Shao, T. Stelzer, P. Torrielli, and M. Zaro, The automated computation of tree-level and next-to-leading order differential cross sections, and their matching to parton shower simulations, J. High Energy Phys. 07 (2014) 079.

[64] Pierre Artoisenet, Rikkert Frederix, Olivier Mattelaer, and Robbert Rietkerk, Automatic spin-entangled decays of heavy resonances in Monte Carlo simulations, J. High Energy Phys. 03 (2013) 015.

[65] E. Boos *et al.*, Generic user process interface for event generators, in *Proceedings of the 2nd Les Houches Workshop on Physics at TeV Colliders* (2001), https://arxiv.org/abs/hep-ph/0109068.

[66] Johan Alwall *et al.*, A standard format for Les Houches event files, Comput. Phys. Commun. **176,** 300 (2007).

[67] Torbjorn Sjostrand, Stephen Mrenna, and Peter Z. Skands, PYTHIA 6.4 physics and manual, J. High Energy Phys. 05 (2006) 026.

[68] Torbjörn Sjöstrand, Stefan Ask, Jesper R. Christiansen, Richard Corke, Nishita Desai, Philip Ilten, Stephen Mrenna, Stefan Prestel, Christine O. Rasmussen, and Peter Z. Skands, An introduction to PYTHIA 8.2, Comput. Phys. Commun. **191,** 159 (2015).

[69] Andy Buckley, Jonathan Butterworth, David Grellscheid, Hendrik Hoeth, Leif Lonnblad, James Monk, Holger Schulz, and Frank Siegert, Rivet user manual, Comput. Phys. Commun. **184,** 2803 (2013).

[70] Christian Bierlich *et al.*, Robust independent validation of experiment and theory: Rivet version 3, SciPost Phys. **8,** 026 (2020).

[71] Matteo Cacciari and Gavin P. Salam, Dispelling the $N^3$ myth for the $k_t$ jet-finder, Phys. Lett. B **641,** 57 (2006).

[72] Matteo Cacciari, Gavin P. Salam, and Gregory Soyez, FastJet user manual, Eur. Phys. J. C **72,** 1896 (2012).

[73] I. Antcheva *et al.*, ROOT: A C++ framework for petabyte data storage, statistical analysis and visualization, Comput. Phys. Commun. **180,** 2499 (2009).

[74] Z. Bern, L. J. Dixon, F. Febres Cordero, S. Höche, H. Ita, D. A. Kosower, and D. Maitre, Ntuples for NLO events at hadron colliders, Comput. Phys. Commun. **185,** 1443 (2014).

[75] G. Bevilacqua, H. B. Hartanto, M. Kraus, and M. Worek, Off-shell top quarks with one jet at the LHC: A comprehensive analysis at NLO QCD, J. High Energy Phys. 11 (2016) 098.

[76] G. Bevilacqua, Heplot (unpublished).

[77] See Supplemental Material at http://link.aps.org/supplemental/10.1103/PhysRevD.105.014018 for the histogram data of all plots as well as input cards for the event generators for reproducibility of our results.

[78] R. V. Harlander, S. Y. Klein, and M. Lipp, FeynGame, Comput. Phys. Commun. **256,** 107465 (2020).

[79] Andrea Banfi, Gavin P. Salam, and Giulia Zanderighi, Infrared safe definition of jet flavor, Eur. Phys. J. C **47,** 113 (2006).

[80] M. Czakon, Flavored jets in top physics and beyond, in *Proceedings of the 14th International Workshop on Top Quark Physics (TOP2021), 2021 (Online workshop)* (2021), https://indico.cern.ch/event/1018454/contributions/4339316/attachments/2308123/3927077/talk.pdf.

[81] Matteo Cacciari, Gavin P. Salam, and Gregory Soyez, The anti-$k_t$ jet clustering algorithm, J. High Energy Phys. 04 (2008) 063.

[82] Sandip Biswas, Kirill Melnikov, and Markus Schulze, Next-to-leading order QCD effects and the top quark mass measurements at the LHC, J. High Energy Phys. 08 (2010) 048.

[83] Gudrun Heinrich, Andreas Maier, Richard Nisius, Johannes Schlenk, and Jan Winter, NLO QCD corrections to $W^+W^-b\bar{b}$ production with leptonic decays in the light of top quark mass and asymmetry measurements, J. High Energy Phys. 06 (2014) 158.

[84] G. Heinrich, Andreas Maier, Richard Nisius, Johannes Schlenk, Markus Schulze, Ludovic Scyboz, and Jan Winter, NLO and off-shell effects in top quark mass determinations, J. High Energy Phys. 07 (2018) 129.

[85] G. Bevilacqua, H. B. Hartanto, M. Kraus, M. Schulze, and M. Worek, Top quark mass studies with $t\bar{t}j$ at the LHC, J. High Energy Phys. 03 (**2018**) 169.

[86] Tomáš Ježo and Paolo Nason, On the treatment of resonances in next-to-leading order calculations matched to a parton shower, J. High Energy Phys. 12 (2015) 065.

[87] Tomáš Ježo, Jonas M. Lindert, Paolo Nason, Carlo Oleari, and Stefano Pozzorini, An NLO + PS generator for $t\bar{t}$ and $Wt$ production and decay including non-resonant and interference effects, Eur. Phys. J. C **76,** 691 (2016).